ORIGINAL ARTICLE

Interplay of tau and functional network connectivity in progressive supranuclear palsy: a [18F]PI-2620 PET/MRI study

Gayane Aghakhanyan[1,2] · M. Rullmann[1] · J. Rumpf[3] · M. L. Schroeter[4] · C. Scherlach[5] · M. Patt[1] · M. Brendel[6] · N. Koglin[7] · A. W. Stephens[7] · J. Classen[3] · K. T. Hoffmann[5] · O. Sabri[1] · H. Barthel[1]

Abstract

Purpose Progressive supranuclear palsy (PSP) is primary 4-repeat tauopathy. Evidence spanning from imaging studies indicate aberrant connectivity in PSPs. Our goal was to assess functional connectivity network alterations in PSP patients and the potential link between regional tau-burden and network-level functional connectivity using the next-generation tau PET tracer [18F]PI-2620 and resting-state functional MRI (fMRI).

Material and methods Twenty-four probable PSP patients (70.9 ± 6.9 years, 13 female), including 14 Richardson syndrome (RS) and 10 non-RS phenotypes, underwent [18F]PI-2620 PET/MRI imaging. Distribution volume ratios (DVRs) were estimated using non-invasive pharmacokinetic modeling. Resting-state fMRI was also acquired in these patients as well as in thirteen older non-AD MCI reference group (64 ± 9 years, 4 female). The functional network was constructed using 141 by 141 region-to-region functional connectivity metrics (RRC) and network-based statistic was carried out (connection threshold $p < 0.001$, cluster threshold pFDR < 0.05).

Results In total, 9870 functional connections were analyzed. PSPs compared to aged non-AD MCI reference group expressed aberrant connectivity evidenced by the significant NBS network consisting of 89 ROIs and 118 connections among them (NBS mass 4226, pFDR < 0.05). Tau load in the right globus pallidus externus (GPe) and left dentate nucleus (DN) showed significant effects on functional network connectivity. The network linked with increased tau load in the right GPe was associated with hyperconnectivity of low-range intra-opercular connections (NBS mass 356, pFDR < 0.05), while the network linked with increased tau load in the left cerebellar DN was associated with cerebellar hyperconnectivity and cortico-cerebellar hypoconnectivity (NBS mass 517, pFDR < 0.05).

Conclusions PSP patients show altered functional connectivity. Network incorporating deep gray matter structures demonstrate hypoconnectivity, cerebellum hyperconnectivity, while cortico-cortical connections show variable changes. Tau load in the right GPe and left DN is associated with functional networks which strengthen low-scale intra-opercular and intra-cerebellar connections and weaken opercular-cerebellar connections. These findings support the concept of tau load-dependent functional network changes in PSP, by that providing evidence for downstream effects of neuropathology on brain functionality in this primary tauopathy.

Keywords [18F]PI-2620 · Functional network connectivity · PET/MRI · Progressive supranuclear palsy · Resting-state functional MRI · Tauopathy

---

O. Sabri and H. Barthel contributed equally to this work.

This article is part of the Topical Collection on Neurology – Movement disorders.

✉ Gayane Aghakhanyan
gayane.aghakhanyan@gmail.com

Extended author information available on the last page of the article

Introduction

Progressive supranuclear palsy (PSP) is the most common primary tauopathy. Tau is encoded by the microtubule-associated protein tau gene and the protein contributes to the stability of the axonal cytoskeleton. The number of spliced copies of the microtubule-binding repeat domain determines whether tau appears as 3-repeat (3R) or a 4-repeat (4R) isoform [1]. In contrast to the 3R/4R tauopathy Alzheimer's

disease, PSP is a "pure 4R tauopathy," where the pathogenic lesions are composed primarily of insoluble 4R tau accumulations. Tau aggregation affects characteristic brain regions leading to diverse but well-defined clinical syndromes [2]. The PSP-Richardson's syndrome (PSP-RS) is the most common phenotype marked by early falls because of postural instability, and by progressive supranuclear vertical gaze palsy [3]. Other common phenotypes associated with PSP pathology include parkinsonism mimicking Parkinson's disease (PSP-P), frontotemporal dementia (PSP-F), and corticobasal syndrome (PSP-CBS) [4].

Structural neuroimaging features such as atrophy of the midbrain, cerebellar peduncles, and of deep gray matter structures, including striatum and thalamus [5, 6], and predominant mid-brain hypometabolism on [18F]FDG PET [7] can be affirmative for PSP. Nevertheless, these biomarkers represent late events in the disease course [8]. Resting-state functional MRI (fMRI) with functional connectivity assessment has also been applied in PSP patients, mainly in PSP-RS phenotype [5]. Most of these resting-state fMRI studies adopted seed-based approaches that require an a priori hypothesis. Others focused on independent component analysis (ICA) [9], providing support for the concept of disrupted and reorganized connectivity in PSP patients [9–11]. However, the network-level analysis that is based on a data-driven hierarchical clustering procedure is still missing in PSP patients. NBS is an alternative method to study brain resting-state functional connectivity and has an advantages compare to other approaches, as it consider the entire brain as an integrated network by using connected graph approach [12]. Furthermore, the NBS enables the higher dimensional analysis compared to other data-driven approaches, such as the low-dimensional ICA. Since tau pathology affects several brain areas in PSP patients, including subcortical structures, cortical and cerebellar regions [13], thus, the NBS approach promises a more comprehensive exploration of whole-brain network connections [14].

In the last few years, progress has been made in the identification and testing of tau PET tracers to image 4R tau occurring in PSP [15]. As such, tau PET has the potential of becoming an imaging biomarker for early diagnosis and disease progression. 4R tau imaging could be used as an outcome measure in clinical treatment trials, particularly those assessing tau-targeted therapies [16]. Among the next-generation tau PET tracers, [18F]PI-2620 has been shown to have a high affinity to recombinant 4R tau fibrils of PSP brain homogenates and no off-target binding to monoamine oxidases [17]. A recent multicenter evaluation by our group showed that [18F]PI-2620 PET imaging corroborates and potentially facilitates a more reliable diagnosis of PSP [18].

The success of tau PET imaging opens new horizons to focus our attention on how regional tau burden can influence the segregation and integration of the passage of neural

information and how the interconnected neuronal network structure of the PSP brain can be affected during the neurodegenerative process. The goal of this study was to explore functional connectivity network alterations in PSP patients applying network-level analysis and to assess the potential link between regional tau burden and functional network-level reorganization using simultaneous acquisition of the next-generation tau PET tracer [18F]PI-2620 and resting-state fMRI on a hybrid PET/MRI system.

Material and methods

Participants

Twenty-four patients (age 70.9 ± 6.9 years, 12 female) with probable PSP according to current diagnostic criteria were included into this retrospective observational study [4]. The PSP cohort consisted of fourteen PSP-RS patients (age 73.1 ± 5.4 years, 6 female) and ten patients with non–RS-variant (age 67.6 ± 7.3 years, 6 female), including predominantly PSPs with parkinsonian presentation (PSP-P), frontal presentation (PSP-F) and with speech/language disorders (PSP-SL). Disease duration was defined as the time between symptom onset and PET/MR imaging. For all PSP patients, we collected the PSP Rating Scale (PSPRS) as a disease severity score [19], the Schwab and England activities of daily living (SEADL) scale for assessment of global functional abilities [20], and the clinical global impression severity (CGI-s) scale for measuring the clinician's view on the patient's global functioning [21].

The resting-state fMRI data of the PSP cohort were compared with those of a non-AD MCI reference group. These were subjects with mild cognitive impairment who were negative on [18F]florbetaben amyloid PET, did not show abnormalities on structural MRI, and who did not progress in terms of their cognitive deficits in clinical follow-up. These were thirteen older non-AD MCI reference group (age 64 ± 9 years, 4 female). Subsidiary analysis was also applied to compare functional network and regional tau burden differences between PSP-RS vs PSP-non-RS patients.

All participants provided written informed consent prior to participating in this study. The data analysis for this retrospective observational study was approved by the local Ethics Committee of the University of Leipzig.

The study cohort demographic details are given in Table 1.

PET/MRI acquisition

Simultaneous PET/MRI acquisition was performed using an integrated 3 T PET/MRI system (Biograph mMR; Siemens, Erlangen, Germany). [18F]PI-2620 PET imaging was

Table 1 Demographics

	CTR N=13	All PSP N=24	p^*	PSP-non-RS N=10	PSP-RS N=14	p°
Age	63.8 (9.1)	70.9 (6.9)	0.03^1	67.7 (7.7)	73.1 (5.4)	0.07^1
Gender			0.3^2			0.24^2
Male	9 (69.2)	11 (45.8)		3 (30%)	8 (57%)	
Female	4 (30.8)	13 (54.2)		7 (70%)	6 (43%)	
PSPRS	–	36.1 (15)		26.0 (7.9)	40.8 (15.4)	0.042^1
SEADL	–	54.7 (23.9)		68.3 (22.3)	48.5 (22.7)	0.092^1
CGI-s	–	4.56 (0.9)		4.0 (0.8)	4.8 (0.9)	0.151^1

If not otherwise noted, data are mean (standard deviation). p^* represent comparison between controls and PSP groups; p° represents comparison between PSP-non-RS and PSP-RS groups. ^{1}Wilcoxon rank sum test, ^{2}Fisher's exact test. Abbreviations: *CGI-s*, clinical global impression severity; *CTR*, controls; *PSP*, progressive supranuclear palsy; *PSPRS*, PSP Rating Scale; *RS*, Richardson syndrome; *SEADL*, Schwab and England activities of daily living

performed in a full dynamic setting (0–60 min post-injection) in 3D list-mode, and reconstructed into a matrix = 256 × 256 (voxel size: $1.00 \times 1.00 \times 2.03$ mm^3) using the built-in ordered subset expectation maximization algorithm with 8 iterations, 21 subsets, and a 3-mm Gaussian filter. Simultaneously to the PET data acquisition, the vendor-provided HiRes attenuation correction MR sequence was obtained. This method combines the individual Dixon attenuation correction approach with a bone attenuation template [22]. Also, a high-resolution 3D T1-weighted image (MP2RAGE) was acquired in each subject for co-registration/anatomical segmentation of the PET and resting-state fMRI data. This was done with the following parameters: 176 contiguous sagittal slices with 1 mm thickness and no gap; repetition time (TR)/echo time (TE) = 5000/2.98 ms; inversion time (TI) = 0 ms; flip angle = 0; field of view = 240 × 256 mm; matrix = 240 × 256; voxel size $1.0 \times 1.0 \times 1.0$ mm. Further, resting-state fMRI data were acquired in 520 echo planar imaging (EPI) volumes with a voxel size of $3 \times 3 \times 4.2$ mm, TR = 2000 ms, TE = 30 ms, flip angle = 90, and slice thickness of 3.5 mm. No task was provided during fMRI scanning. Patients were instructed to keep the eyes open without fixation during the resting-state fMRI acquisition.

Image processing

Region of interest identification

Cortical and subcortical regions of interests (ROIs) were generated on the MP2RAGE MRIs from anatomical regions labeled by atlases (in total 141 ROIs). For resting-state fMRI analysis, 130 ROIs have been selected from the default CONN atlas, which is a combination of the FSL Harvard–Oxford cortical atlas for cortical and subcortical areas [23] and Automated Anatomical Labeling atlas (AAL116) for cerebellar areas [24]. Additional eleven ROIs were included from the atlas of the Basal Ganglia (ATAG) [25],

including periaqueductal gray (PAG) and bilateral globus pallidus externus (GPe), subthalamic nucleus (STN), substantia nigra (SN), red nucleus (RN), and cerebellar dentate nucleus (DN) from the Probabilistic cerebellar atlas [26]. For calculating mean DVR values of the [^{18}F]PI-2620, fifteen tau-in-PSP regions (according to Kovacs et al. [13]) were selected using ATAG atlas [25], including bilateral striatum, GPe, globus pallidus internus (GPi), STN, SN, RN, and cerebellar DN from Probabilistic cerebellar atlas [26].

[^{18}F]PI-2620 PET data analysis

The dynamic [^{18}F]PI-2620 PET datasets were motion-corrected using the individual summed 0–4.5-min frames as reference after co-registration of the reference to the individual MR data in PMOD (version 3.5, PMOD Technologies LLC, Zurich, Switzerland). Automatized brain normalization settings in PMOD included nonlinear warping, 8-mm input smoothing, equal modality, 16 iterations, frequency cut-of 3, regularization 1.0, and no thresholding. The transformation was saved and applied to the full dynamic [^{18}F]PI-2620 PET datasets to minimize interpolation. Distribution volume ratios (DVRs) were estimated using non-invasive pharmacokinetic modeling (MRTM2 [27] in PMOD) with lower cerebellum as reference region [18]. To ascertain that the tau-in-PSP DVRs in PSP patients fall into pathological range, we calculated DVR z-scores using the mean and standard deviation (SD) of an in-house [^{18}F]PI-2620 normal dataset consisted of ten healthy controls (2 men; mean ± SD age of 67 ± 7 years). The details about the [^{18}F]PI-2620 normal dataset are provided elsewhere [18].

Resting-state fMRI

Resting-state fMRI processing was done using Statistical Parametric Mapping (SPM) software, version 12 (Wellcome Trust Centre for Neuroimaging, UCL, London, UK)

(https://www.fil.ion.ucl.ac.uk/spm/software/spm12/) and CONN toolbox, version 18a (https://web.conn-toolbox.org). CONN is a Matlab-based cross-platform software (embedded with SPM12) for computation, display, and analysis of functional connectivity MRI. It covers the entire pipeline from raw fMRI data to hypothesis testing [28]. The toolbox implements the component-based noise correction method (Comp-Cor) strategy for physiological and other noise source reduction, additional removal of movement, and temporal covariates, temporal filtering and windowing of the residual BOLD contrast signal, first-level estimation of multiple standard functional connectivity measures, and second-level random effect analysis for resting-state data. We followed the default preprocessing pipeline. Images were realigned and unwarped. Slice-timing was corrected in ascending order using SPM12 procedure. For functional outlier detection, we used intermediate settings (97th percentile in normative sample) and acquisitions with frame-wise displacement above 0.9 mm or global BOLD signal changes above 5 s.d. are flagged as potential outliers. Both functional data and structural data were segmented to gray matter, white matter, and cerebrospinal fluid and normalized to MNI coordinates. Functional images were smoothed to 8-mm full width at half maximum (FWHM) Gaussian kernel. Subsequently, denoising was performed by default, including temporal band-pass filtering (below 0.008 Hz and above 0.09 Hz) and linear regression.

Functional network construction

Functional brain networks were constructed using 141 by 141 ROI-to-ROI functional connectivity metrics (RRC), which represent the connectivity between all pairs of ROIs among a pre-defined set of ROIs. The definition of these metrics follows exactly the same organization and properties as the seed-based connectivity measures but avoids the asymmetry between seeds (ROIs) and targets (voxels). These metrics are often used when researchers are interested in the simultaneously study of entire networks of connections [28].

Network analysis

To study the network-based inferences, we used network-based statistic (NBS), which allows to make inferences about entire networks of ROIs [29]. NBS is a nonparametric cluster-level statistics technique based on the graph theoretical concept of connected components. We first created a two-dimensional statistical parametric map based on the ROI-to-ROI matrix of T-statistics that were estimated using a general linear model (GLM). This statistical parametric map was then thresholded using a connection threshold $p < 0.001$. The resulting suprathreshold connections defined a graph among all remaining ROIs that survived thresholding. This graph was then broken down into components, defined as connected subgraphs. Each network was then characterized by its network mass (sum of T-squared statistics over all connections within each cluster), and these values were compared to a distribution of expected network mass values under the null hypothesis, which was numerically estimated using 10,000 permutation iterations of the original data. NBS was chosen given its advantage of rejecting the null hypothesis at the network levels. This allowed to observe the effect of significant network clusters rather than significant individual connections.

Statistics

All statistical analyses were performed in R (R Core Team, 2018) and in MATLAB 2018a (The Mathworks Inc., 2018). The Kruskal–Wallis rank sum test was used for testing age differences between three groups, the Fisher's exact test for testing gender differences between groups, and the Wilcoxon rank sum test for testing differences between two groups (PSP-RS and PSP-non-RS). For network-level statistics, first, general linear model (GLM, implemented in CONN toolbox) was designed for each connection using one-way ANCOVA with covariate control for between-subjects contrast (PSP vs non-AD MCI reference group; PSP-RS vs PSP-non-RS) and age/sex as a nuisance covariates. Similarly, for testing the effect of regional DVRs on functional network, a multiple regression at fix level of age/sex effects was modeled to account for age- and sex-related variabilities. For each model (ANCOVA or multiple regression), the GLM estimated entire ROI-to-ROI matrix of T-statistics resulting in a two-dimensional statistical parametric map, which was further thresholded at a connection threshold $p < 0.001$ and utilized for NBS with 10,000 permutation to control the rate of falsely detecting networks at pFDR < 0.05. The T-statistics for connections that construct the significant network were reported.

Results

PSP patients

Fourteen out of the twenty-four PSP patients had PSP-RS phenotype (58%) with a mean PSPRS value of 41 ± 15, a mean SEADL value of 48 ± 23, and CGI-s score of 4.8 ± 0.9. The ten patients (42%) with PSP-non-RS forms had a mean PSPRS value of 26 ± 8, mean SEADL value of 68 ± 22, and CGI-s score of 4.0 ± 0.8. The PSPRS score of PSP-RS and PSP-non-RS patients differed significantly ($p < 0.05$), with higher values in PSP-RS patients (Table 1). The SEADL and CGI-s scores show no significant differences between PSP-RS and non-RS phenotypes. The PSP-RS patients were

relatively older compared to PSP-non-RS group with borderline statistical significant ($p = 0.07$). No significant gender difference was found between PSP-RS and PSP-non-RS groups ($p = 0.24$).

[^{18}F]PI-2620 binding

The PSP patients demonstrated high specific [^{18}F]PI-2620 binding in the PSP target regions, including GPe and GPi, ST, STN, RD, and cerebellar DN. Table 2 depicts regional [18F]PI-2620 DVRs and *z*-scores in the PSP target regions. The highest non-displaceable DVRs were revealed in the bilateral GPe/GPi and DN both for PSP-RS and non-RS phenotypes (Table 2). No significant [^{18}F]PI-2620 binding differences among PSP-RS and PSP-non-RS groups were observed for all subcortical PSP target regions, both for left (L) and right (R) hemisphere (Table 2).

Functional network connectivity

In total, 9870 functional connections among 141 ROIs were analyzed. PSP patients, compared to non-AD MCI reference group, expressed altered whole-brain functional network connectivity (NBS mass = 4350, pFDR < 0.05) (Fig. 1). The network consisted of 89 ROIs, including cortical, subcortical, and cerebellar nodes, and 118 connections among them. Details about single connections which the network is comprised of with corresponding *T*-statistics are presented in the Supplement (Table S1). In addition, histograms of

the Cohen's *d* effect sizes with confidence intervals for each connection in the NBS network are depicted in the Supplement (Fig. S1).

Cortical nodes showed variable changes (hyper- and hypoconnectivity) with other nodes. Lower connectivity was observed between large-scale cortico-cortical circuits including auditory cortex, and nodes embedded in the default mode network and salience network. The secondary visual cortex showed increased connectivity with inferior temporal gyrus, while motor and frontal-parietal control networks showed decreased long-range connectivity. Interestingly, the cerebellum showed apparent hyperconnectivity with cortical associative nodes, and lower connectivity with the GPe, brainstem, and limbic cortex (including the hippocampus, parahippocampal gyrus, and amygdala) (Fig. 1). The subcortical structures were characterized by cortical and cerebellar hypoconnectivity.

The subsidiary analysis for comparing functional network-level interference between PSP-RS and PSP-non-RS patients revealed no significant differences.

Effect of tau PET signals on network connectivity

In the PSP group, the [^{18}F]PI-2620 DVRs in the right GPe and left DN had significant effects on functional network connectivity. The network linked with increased [^{18}F]PI-2620 DVRs of the right GPe consisted of 9 ROIs and 10 connections among them (NBS mass 356, pFDR < 0.05) and was associated with hyperconnectivity of low-range

Table 2 [^{18}F]PI-2620 tau PET distribution volume ratios and *z*-scores in PSP target regions

	PSP-non-RS		PSP-RS		*p*
	DVR	*z*-score	DVR	*z*-score	
	N = 10		*N* = 14		
Globus pallidus external l	1.40 (0.13)	2.29	1.40 (0.13)	2.35	0.912
Globus pallidus external r	1.44 (0.12)	2.64	1.40 (0.13)	2.23	0.469
Globus pallidus internal l	1.34 (0.11)	2.6	1.36 (0.15)	2.86	0.697
Globus pallidus internal r	1.43 (0.14)	2.98	1.37 (0.14)	2.42	0.363
Periaqueductal gray area	1.03 (0.13)	1.04	0.98 (0.13)	0.98	0.398
Red nucleus l	1.27 (0.12)	1.05	1.24 (0.16)	0.8	0.649
Red nucleus r	1.34 (0.14)	1.38	1.27 (0.15)	0.75	0.294
Substantia nigra l	1.35 (0.21)	2.1	1.30 (0.24)	1.5	0.585
Substantia nigra r	1.39 (0.23)	1.94	1.27 (0.21)	1.5	0.182
Subthalamic nucleus l	1.35 (0.10)	2.1	1.38 (0.12)	2.39	0.550
Subthalamic nucleus r	1.38 (0.16)	2.67	1.35 (0.15)	2.37	0.671
Striatum l	1.18 (0.11)	1.22	1.19 (0.08)	1.38	0.776
Striatum r	1.18 (0.09)	1.32	1.19 (0.09)	1.42	0.849
Dentate nucleus l	1.32 (0.13)	3.64	1.29 (0.13)	2.8	0.581
Dentate nucleus r	1.33 (0.14)	3.88	1.31 (0.12)	3.1	0.624

DVRs are mean (standard deviation). *z*-scores are mean as calculated by comparison with a normal dataset. *z*-scores ≥ 2 indicate 2 standard deviation above the mean of normal population. Abbreviations: *l*, left; *PSP*, progressive supranuclear palsy; *r*, right; *RS*, Richardson syndrome

Fig. 1 Connectome rings representing a significant NBS network between PSP patients and non-AD MCI reference group (NBS mass 4225, connection threshold $p < 0.001$, cluster threshold pFDR < 0.05) using 141 by 141 RRC matrices. The cluster is comprised of 89 ROIs and 118 connections among them. Abbreviations: AC, cingulate gyrus, anterior division; AG, angular gyrus; aITG, inferior temporal gyrus, anterior division; aMTG, middle temporal gyrus, anterior division; aPaHC, parahippocampal gyrus, anterior division; aPaHC, parahippocampal gyrus, anterior division; aSMG, supramarginal gyrus, anterior division; aSTG, superior temporal gyrus, anterior division; Cereb, cerebellum; CO, central opercular cortex; FO, frontal operculum cortex; FOrb, frontal orbital cortex; FP, frontal pole; GPe, globus pallidus externus; HG, Heschl's gyrus; IC, insular cortex; ICC, intracalcarine cortex; IFG tri, inferior frontal gyrus, pars triangula-

ris; iLOC, lateral occipital cortex, inferior division; l, left; MedFC, frontal medial cortex; MidFG, middle frontal gyrus; OFusG, occipital fusiform gyrus; PaCiG, paracingulate gyrus; PAG, periaqueductal gray; pITG, inferior temporal gyrus, posterior division; pMTG, middle temporal gyrus, posterior division; PostCG, postcentral gyrus; PP, planum polare; pPaHC, parahippocampal gyrus, posterior division; pPaHC, parahippocampal gyrus, posterior division; PreCG, precentral gyrus; pSMG, supramarginal gyrus, posterior division; pSTG, superior temporal gyrus, posterior division; PT, planum temporale; Put, putamen; r, right; RedN, red nucleus; SCC, supracalcarine cortex; SFG, superior frontal gyrus; SMA, supplementary motor cortex; SubCalC, subcallosal cortex; TOFusC, temporal occipital fusiform cortex; oMTG, middle temporal gyrus, temporooccipital part; TP, temporal pole; Ver, vermis

intra-opercular connections, including bilateral frontal/parietal opercular and temporal polar regions (Fig. 2). Details about single connections which the network is comprised of with corresponding *T*-statistics are presented in Table 3A.

The network linked with increased [^{18}F]PI-2620 DVRs of the left cerebellar DN consisted of 13 ROIs and 12

connections among them (NBS mass 517, pFDR < 0.05), and was associated with cerebellar hyperconnectivity and cortico-cerebellar hypoconnectivity (Fig. 3). Details about single connections the network is comprised of with corresponding *T*-statistics are presented in Table 3B.

Fig. 2 Connectome rings representing a significant NBS network in PSP patients in association with [18F]PI-2620 DVRs in the right GPe (NBS mass 356, connection threshold $p < 0.001$, cluster threshold pFDR < 0.05). Note, hyperconnectivity of low-scale opercular connections including bilateral frontal/parietal operculum and temporal pole in association with increased [18F]PI-2620 DVRs in the right GPe. Abbreviations: aPHC, parahippocampal gyrus, anterior division; CO, central opercular cortex; GPe, globus pallidus externus; FO, frontal opercular cortex; IC, insular cortex; NBS, network-based statistics; PO, parietal opercular cortex; PP, planum polare; pSTG, superior temporal gyrus, posterior division

Discussion

We applied a network-based approach to study resting-state brain functional connectivity and the network-level changes in PSP patients. We further attempted to link functional network with subcortical [18F]PI-2620 binding in PSP patients. First, we provide evidence for a functional connectivity network alteration within large-scale nodal connections in PSP, which mainly manifested as increased functional connectivity within cortico-cerebellar brain circuits, and decreased connectivity between cortico-cortical, cortico-subcortical, and subcortical-cerebellar circuits. Next, we determined that tracer binding in the right GPe and left DN was associated with certain functional network alteration patterns.

Over the last decade, brain functional connectivity has gained much interest and has been extensively studied in neurodegenerative disorders, including PSP [9–11, 30, 31]. Recently neurodegenerative diseases even have been conceptualized as "molecular nexopathies," where changes in brain connectivity are related to specific molecular changes [32]. PSP seems to be a paradigmatic disease and in our study, we were able assess the interaction between brain

network alterations as investigated with resting-state fMRI and molecular underpinnings as measured with tau-PET. To the best of our knowledge, the network-level analysis using RRC matrices as defined by a data-driven hierarchical clustering procedure [28] and interpolating NBS without a priori hypotheses has not been yet adopted to investigate resting-state functional connectivity in PSP patients. Our findings that PSP patients, compared to non-AD MCI reference group, express aberrant network-level connectivity are largely consistent with others that have explored the resting-state connectivity with different means [9, 30]. PSP-associated neurodegeneration was attributed to both decreased and increased functional connectivity, suggesting that the decreased functional connectivity is linked to neurodegenerative phenomena, while an increased functional connectivity is probably due to adaptive changes [31]. Similarly, we observed lower connectivity between large-scale cortico-cortical circuits including nodes within the default mode network and salience network that probably reflects the disruption of those networks and their functional failure. On the other hand, the secondary visual cortices exhibited hyperconnectivity with the inferior temporal cortex, which is a key

Table 3 Effect of tau PET readouts on functional network connectivity

Connection	ROI 1	ROI 2	T-statistics
A. Network connections in association with DVR of the right GPe			
1	Planum polare right	Insular cortex right	4.58
2	Planum polare left	Parietal operculum cortex right	4.55
3	Planum polare right	Parietal operculum cortex left	4.54
4	Frontal operculum cortex right	Planum polare right	4.53
5	Planum polare left	Central opercular cortex left	4.21
6	Frontal operculum cortex right	Planum polare left	4.06
7	Planum polare right	Operculum cortex right	3.95
8	Central opercular cortex left	Superior temporal gyrus, posterior division right	3.92
9	Superior temporal gyrus, posterior division right	Parahippocampal gyrus, anterior division left	3.87
10	Planum polare left	Superior temporal gyrus, posterior division right	3.83
B. Network connections in association with DVR of left DN			
1	Inferior temporal gyrus, temporooccipital part right	Cerebellum crus 1 left	5.64
2	Cerebellum 10 left	Vermis 8	5.1
3	Cerebellum 10 left	Vermis 7	4.95
4	Cerebellum 10 left	Cerebellum 6 left	4.94
5	Inferior temporal gyrus, temporooccipital part right	Vermis 8	4.88
6	Parietal operculum cortex right	Cerebellum 6 right	−4.77
7	Planum polare right	Cerebellum 10 left	4.66
8	Temporal fusiform cortex, posterior division left	Cerebellum 10 left	4.32
9	Central opercular cortex left	Vermis 6	−4.05
10	Parietal operculum cortex right	Cerebellum 6 left	−4.03
11	Cerebellum 10 left	Cerebellum 8 left	4.01
12	Cerebellum 10 left	Vermis 6	3.99

Single ROI-to-ROI connections and associated T-statistics are provided that construct the significant network. (A) Network connections in association with distribution volume ratios (DVR) of the right globus pallidus externus (GPe). The cluster comprises 9 ROIs and 10 connections among them (NBS mass 356, pFDR < 0.05). (B) Network connections in association with DVR of the left cerebellar dentate nucleus (DN). The cluster comprises 13 ROIs and 12 connections among them (NBS mass 517, pFDR < 0.05)

part of the ventral visual pathway implicated in object, face, and scene perception [33]. Visual dysfunction and altered visual perception are common features in PSP patients and enhanced visual network oscillations might represent an adaptive shift in cortico-cortical network architecture.

It has been hypothesized that clinical manifestations in PSP might result from the degeneration of deep gray matter structures, consequently disrupting cortico-subcortical brain circuits [34]. Reinforcing this idea, we observed decreased deep gray matter connectivity with cortical regions as well as with brainstem, cerebellum, and limbic cortex. It seems that basal ganglia, where tau pathology is most prominent in PSP [13], display lower functional connectivity with cortical regions implying that the tau proteinopathy leads to neurodegeneration inducing large-scale functional network degradation and disintegration.

Similarly, the cerebellum showed lower connectivity with the deep gray matter, brainstem, and limbic cortex. Intense hyperconnectivity was observed with superior and inferior temporal gyrus, supplementary motor cortex, auditory, and primary visual cortex. It has been demonstrated in PSP that tau accumulates in the somata and dendrites of Purkinje cells of the cerebellar cortex, as well as focal tau filaments in the radial processes of Bergmann's glia and cerebellar deep nuclei (in addition to the extra-cerebellar brain regions involved in this disorder) [35]. However, the cerebellar cortex shows functional resistance to tau pathology that might be translated into the ability of the cerebellar cortex being largely connected with other brain regions, to enhance network architecture and functional interaction. It is known that the cerebellum contributes to several motor and non-motor functions [36]. Hence, to clarify whether and how functional deficits underly increased functional connectivity within the frontal-cerebellar circuits in PSP requires further research.

With the availability of appropriate tau PET tracers, it is now possible to study the direct consequence of tau proteinopathy on brain connectivity in vivo in PSP. We strongly believe that understanding whether and how multimodal neuroimaging markers are related to each other is a crucial next step for PSP research. The topographical similarities and spatial correspondence between tau pathology and brain networks have been recently addressed in AD

Fig. 3 Connectome rings representing a significant NBS network in PSP patients in association with [18F]PI-2620 DVRs in the left cerebellar dentate nucleus (mass 517, connection threshold $p < 0.001$, cluster threshold pFDR < 0.05). Note, the low-scale intra-cerebellar and ITG-cerebellar hyper-connectivity, and opercular-cerebellar hypoconnectivity. Abbreviations: CO, central opercular cortex; ITG, inferior temporal gyrus; pITG, inferior temporal gyrus, posterior division; PO, parietal opercular cortex; pTFusC, temporal fusiform cortex, posterior division; toITG, inferior temporal gyrus, temporooccipital part

Network associated with tau load in the left DN
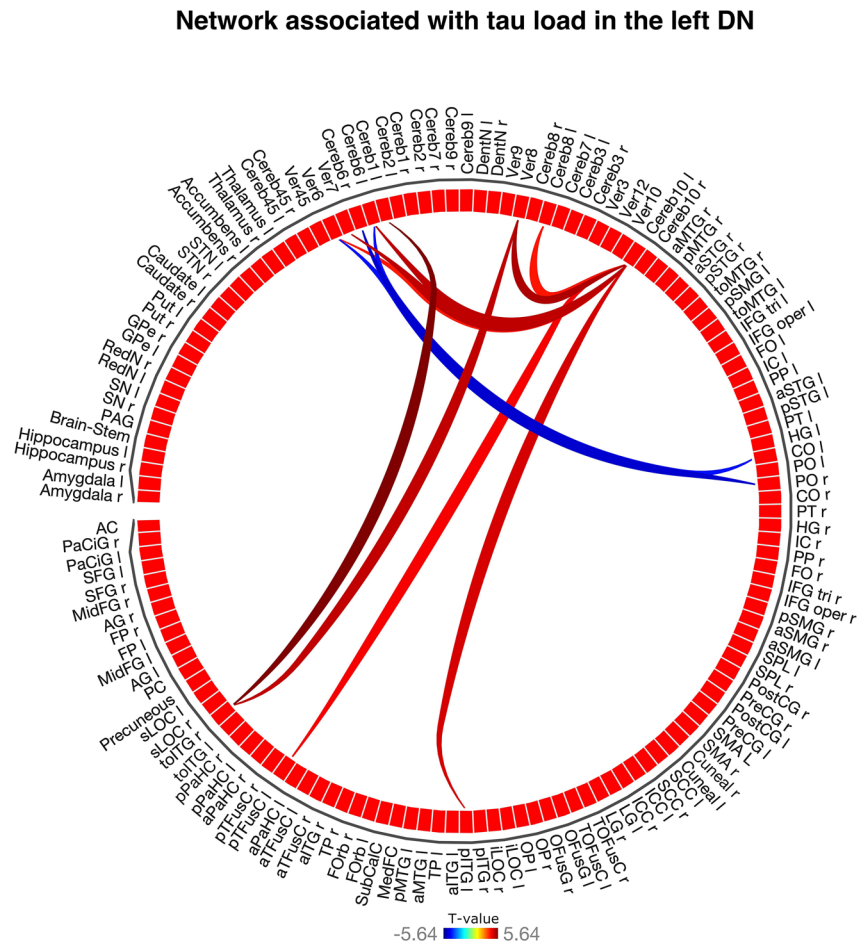
and a small PSP cohort [37] using [18F]AV-1451 ([18F]flortaucipir). However, many of the regions of interest in PSP largely coincide with areas showing off-target binding for [18F]flortaucipir (i.e., to monoamine oxidase, MAO-B, in the basal ganglia) [38]. Besides, growing evidence confirms that [18F]flortaucipir should not be clinically used to image tauopathies other than AD [39]. In our study, we utilized the next-generation tau PET tracer [18F]PI-2620 which has lower off-target binding [18].

As a consequence of tau pathology in the subcortical PSP target regions, the overall network connectivity seems to be reorganized. In particular, we found that the [18F]PI-2620 binding in the right GPe is strongly associated with hypoconnectivity within the low-scale frontotemporoparietal opercular network, while the [18F]PI-2620 binding in the left DN is linked to low-scale intra-cerebellar network hyperconnectivity and large-scale cortico-cerebellar hypoconnectivity. The GPe and cerebellar DN have a putative role in the pathophysiology of PSP and reflect those brain regions that are severely affected in post-mortem specimens [3]. With increased level of tau, the cortico-cerebellar connections seem to be strengthened, while predominantly

cortical-cortical connections are weakened. This phenomenon, together with short-range intra-cerebellar hyperconnectivity, might be a rendition of the loss of network specialization in PSP patients that may contribute to the generalized spread of neuronal activity, abnormal oscillations, and abnormal synchronization [40], but on the other hand, it may represent a plasticity-related shift in neuronal activity from atrophic to intact brain structures, as deep structures can no longer sustain adequate information transfer [41].

Limitations of our study are its cross-sectional design and the limited number of patients. The latter did not permit designing a study under the perspective of different PSP phenotypes. Instead, we grouped all PSP patients of subtypes other than RS into a PSP-non-RS sub-cohort. As we did not find differences in the subcortical tau tracer binding between the PSP-RS and non-RS phenotypes, we pooled the data for the tau PET vs resting-state fMRI association analyses. Additional studies in larger PSP cohorts are needed to test whether the reported tau PET signal vs functional network connectivity associations differ between different PSP phenotypes. In addition, the reference group against which the resting-state fMRI data of

the PSP patients were compared in this study comprised MCI subjects who were amyloid-negative in PET imaging as done of the same hybrid PET/MRI system as used in this present study. This, by definition, excludes AD as underlying disorder. However, we cannot exclude other dementia disorders causing the MCI in these subjects. One might argue that our reference group better reflects a real-world clinical scenario (especially as PSP can represent with cognitive despite the leading motor symptoms) than using healthy controls. However, we plan in future work to reproduce our findings comparing PSP patients also with healthy controls in a prospective manner.

In conclusion, employing simultaneous [^{18}F]PI-2620 tau PET/resting-state fMRI to study functional network connectomics and network-level reorganization in relation to subcortical tau load in PSP patients, we show that PSP patients have altered functional connectivity that operates within large- and short-scale neuronal network levels. Tau tracer binding in the bilateral GPe and left cerebellar DN is related to remodeled functional connectivity with strengthened opercular and cerebellar inter-connections and weakened large-scale cortico-cerebellar and cortico-cortical networks. These results support the concept of functional network changes in PSP in response to tau pathology and motivate future investigations in a larger PSP cohort. Here, it will be interesting to study how these findings potentially improve disease progression prediction/monitoring.

Declarations

References

1. Goedert M, Spillantini MG. Pathogenesis of the tauopathies. J Mol Neurosci: MN. 2011;45:425–31.
2. VandeVrede L, Ljubenkov PA, Rojas JC, et al. Four-repeat tauopathies: current management and future treatments. Neurotherapeutics. 2020;17:1563–1581. https://doi.org/10.1007/s13311-020-00888-5.
3. Williams DR, Lees AJ. Progressive supranuclear palsy: clinico-pathological concepts and diagnostic challenges. Lancet Neurol. 2009;8:270–9.
4. Höglinger GU, Respondek G, Stamelou M, Kurz C, Josephs KA, Lang AE, et al. Clinical diagnosis of progressive supranuclear palsy: the movement disorder society criteria. Mov Disord: Off J Mov Disord Soc. 2017;32:853–64.
5. Whitwell JL, Höglinger GU, Antonini A, Bordelon Y, Boxer AL, Colosimo C, et al. Radiological biomarkers for diagnosis in PSP: where are we and where do we need to be? Mov Disord: Off J Mov Disord Soc. 2017;32:955–71.
6. Albrecht F, Bisenius S, Neumann J, Whitwell J, Schroeter ML. Atrophy in midbrain & cerebral/cerebellar pedunculi is characteristic for progressive supranuclear palsy – a double-validation whole-brain meta-analysis. NeuroImage: Clinical. 2019;22:101722.
7. Beyer L, Meyer-Wilmes J, Schönecker S, Schnabel J, Brendel E, Prix C, et al. Clinical routine FDG-PET imaging of suspected progressive supranuclear palsy and corticobasal degeneration: a gatekeeper for subsequent tau-PET imaging? Front Neurol. 2018;9:483.
8. Zhao P, Zhang B, Gao S, Li X. Clinical, MRI and 18F-FDG-PET/CT analysis of progressive supranuclear palsy. J Clin Neurosci. 2020;80:318–23.
9. Bharti K, Bologna M, Upadhyay N, Piattella MC, Suppa A, Petsas N, et al. Abnormal resting-state functional connectivity in progressive supranuclear palsy and corticobasal syndrome. Front Neurol. 2017;8:1247.
10. Piattella MC, Tona F, Bologna M, Sbardella E, Formica A, Petsas N, et al. Disrupted resting-state functional connectivity in progressive supranuclear palsy. Am J Neuroradiol. 2015;36:915–21.
11. Whitwell JL, Avula R, Master A, Vemuri P, Senjem ML, Jones DT, et al. Disrupted thalamocortical connectivity in PSP: a resting-state fMRI, DTI, and VBM study. Parkinsonism Relat Disord. 2011;17:599–605.
12. Bullmore E, Sporns O. Complex brain networks: graph theoretical analysis of structural and functional systems. Nat Rev Neurosci. 2009;10:186–98.

13. Kovacs GG, Lukic MJ, Irwin DJ, Arzberger T, Respondek G, Lee EB, et al. Distribution patterns of tau pathology in progressive supranuclear palsy. Acta Neuropathol. 2020;140:99–119 (Springer Berlin Heidelberg).

14. Smith SM, Vidaurre D, Beckmann CF, Glasser MF, Jenkinson M, Miller KL, et al. Functional connectomics from resting-state fMRI. Trends Cogn Sci. 2013;17:666–82.

15. Schöll M, Maass A, Mattsson N, Ashton NJ, Blennow K, Zetterberg H, et al. Biomarkers for tau pathology. Mol Cell Neurosci. 2019;97:18–33.

16. Whitwell JL. Tau imaging in parkinsonism: what have we learned so far? Mov Disord Clin Pract. 2018;5:118–30.

17. Kroth H, Oden F, Molette J, Schieferstein H, Capotosti F, Mueller A, et al. Discovery and preclinical characterization of [18F] PI-2620, a next-generation tau PET tracer for the assessment of tau pathology in Alzheimer's disease and other tauopathies. Eur J Nucl Med Mol Imaging. 2019;46:2178–89.

18. Brendel M, Barthel H, van Eimeren T, et al. Assessment of 18F-PI-2620 as a Biomarker in Progressive Supranuclear Palsy. JAMA Neurol. 2020;77(11):1408–1419. https://doi.org/10.1001/jamaneurol.2020.2526.

19. Golbe LI, Ohman-Strickland PA. A clinical rating scale for progressive supranuclear palsy. Brain. 2007;130:1552–65.

20. Schwab RS, England AC. Projection technique for evaluating surgery in Parkinson's disease. In: Billingham FH, Donaldson MC, editors. Third symposium on Parkinson's disease. Edinburgh: Churchill Livingstone; 1969. p. 152–7.

21. Guy W. ECDEU assessment manual for psychopharmacology, Revised. US Department of Health, Education, and Welfare Publication (ADM). Rockville: National Institute of Mental Health. 1976. p. 76–338.

22. Ladefoged CN, Law I, Anazodo U, St Lawrence K, Izquierdo-Garcia D, Catana C, et al. A multi-centre evaluation of eleven clinically feasible brain PET/MRI attenuation correction techniques using a large cohort of patients. Neuroimage. 2017;147:346–59.

23. Makris N, Goldstein JM, Kennedy D, Hodge SM, Caviness VS, Faraone SV, Tsuang MT, Seidman LJ. Decreased volume of left and total anterior insular lobule in schizophrenia. Schizophr Res. 2006;83(2–3):155–71.

24. Tzourio-Mazoyer N, Landeau B, Papathanassiou D, Crivello F, Étard O, Delcroix N, Mazoyer B, Joliot M. Automated anatomical labeling of activations in SPM using a macroscopic anatomical parcellation of the MNI MRI single-subject brain. Neuroimage. 2002;15:273–89.

25. Keuken MC, Forstmann BU. A probabilistic atlas of the basal ganglia using 7 T MRI. Data Brief. 2015;4:577–82.

26. Diedrichsen J, Balsters JH, Flavell J, Cussans E, Ramnani N. A probabilistic MR atlas of the human cerebellum. NeuroImage. 2009;46:39–46 (Elsevier B.V.).

27. Ichise M, Liow J-S, Lu J-Q, Takano A, Model K, Toyama H, et al. Linearized reference tissue parametric imaging methods: application to [11C]DASB positron emission tomography studies of the serotonin transporter in human brain. J Cereb Blood Flow Metab. 2003;23:1096–112.

28. Whitfield-Gabrieli S, Nieto-Castanon A. Conn: a functional connectivity toolbox for correlated and anticorrelated brain networks. Brain Connect. 2012;2:125–41.

29. Zalesky A, Fornito A, Bullmore ET. Network-based statistic: identifying differences in brain networks. NeuroImage. 2010;53:1197–207 (Elsevier Inc.).

30. Gardner RC, Boxer AL, Trujillo A, Mirsky JB, Guo CC, Gennatas ED, et al. Intrinsic connectivity network disruption in progressive supranuclear palsy. Ann Neurol. 2013;73:603–16.

31. Rosskopf J, Gorges M, Müller H-P, Lulé D, Uttner I, Ludolph AC, et al. Intrinsic functional connectivity alterations in progressive supranuclear palsy: differential effects in frontal cortex, motor, and midbrain networks. Mov Disord: Off J Mov Disord Soc. 2017;32:1006–15.

32. Warren JD, Rohrer JD, Schott JM, Fox NC, Hardy J, Rossor MN. Molecular nexopathies: a new paradigm of neurodegenerative disease. Trends Neurosci. 2013;36:561–9.

33. Conway BR. The organization and operation of inferior temporal cortex. Annu Rev Vis Sci. 2018;4:381–402.

34. Abos A, Segura B, Baggio HC, Campabadal A, Uribe C, Garrido A, et al. Disrupted structural connectivity of fronto-deep gray matter pathways in progressive supranuclear palsy. Neuroimage Clin. 2019;23:101899.

35. Piao Y-S, Hayashi S, Wakabayashi K, Kakita A, Aida I, Yamada M, et al. Cerebellar cortical tau pathology in progressive supranuclear palsy and corticobasal degeneration. Acta Neuropathol. 2002;103:469–74.

36. Voogd J. The human cerebellum. J Chem Neuroanat. 2003;26:243–52.

37. Cope TE, Rittman T, Borchert RJ, Jones PS, Vatansever D, Allinson K, et al. Tau burden and the functional connectome in Alzheimer's disease and progressive supranuclear palsy. Brain. 2018;141:550–67.

38. Murugan NA, Chiotis K, Rodriguez-Vieitez E, et al. Cross-interaction of tau PET tracers with monoamine oxidase B: evidence from in silico modelling and in vivo imaging. Eur J Nucl Med Mol Imaging. 2019;46:1369–1382. https://doi.org/10.1007/s00259-019-04305-8.

39. Barthel H. First tau PET tracer approved: toward accurate in vivo diagnosis of Alzheimer disease. J Nucl Med. 2020;61:1409–10.

40. Galvan A, Devergnas A, Wichmann T. Alterations in neuronal activity in basal ganglia-thalamocortical circuits in the parkinsonian state. Front. Neuroanat. 2015;9:5. https://doi.org/10.3389/fnana.2015.00005.

41. Rytty R, Nikkinen J, Paavola L, Abou Elseoud A, Moilanen V, Visuri A, Tervonen O, Renton AE, Traynor BJ, Kiviniemi V, Remes AM. GroupICA dual regression analysis of resting state networks in a behavioral variant of frontotemporal dementia. Front Hum Neurosci. 2013;7:461. https://doi.org/10.3389/fnhum.2013.00461.

Authors and Affiliations

Gayane Aghakhanyan[1,2] ⬤ · M. Rullmann[1] · J. Rumpf[3] · M. L. Schroeter[4] · C. Scherlach[5] · M. Patt[1] · M. Brendel[6] · N. Koglin[7] · A. W. Stephens[7] · J. Classen[3] · K. T. Hoffmann[5] · O. Sabri[1] · H. Barthel[1]

1   Department of Nuclear Medicine, University of Leipzig, Leipzig, Germany

2   Department of Translational Research and of New Surgical and Medical Technologies, University of Pisa, Pisa, Italy

3   Department of Neurology, University of Leipzig, Leipzig, Germany

4   Max Planck Institute for Human Cognitive and Brain Sciences & Clinic for Cognitive Neurology, University of Leipzig, Leipzig, Germany

5   Department of Neuroradiology, University of Leipzig, Leipzig, Germany

6   Department of Nuclear Medicine, University Hospital of Munich, LMU Munich, Munich, Germany

7   Life Molecular Imaging GmbH, Berlin, Germany